

REPORT DOCUMENTATION PAGE				Form Approved OMB No. 0704-0188	
Public reporting burden for this collection of information is estimated to average 1 hour per response, including the time for reviewing instructions, searching existing data sources, gathering and maintaining the data needed, and completing and reviewing this collection of information. Send comments regarding this burden estimate or any other aspect of this collection of information, including suggestions for reducing this burden to Department of Defense, Washington Headquarters Services, Directorate for Information Operations and Reports (0704-0188), 1215 Jefferson Davis Highway, Suite 1204, Arlington, VA 22202-4302. Respondents should be aware that notwithstanding any other provision of law, no person shall be subject to any penalty for failing to comply with a collection of information if it does not display a currently valid OMB control number. PLEASE DO NOT RETURN YOUR FORM TO THE ABOVE ADDRESS.					
1. REPORT DATE (DD-MM-YYYY) 20-06-1999		2. REPORT TYPE Technical Paper		3. DATES COVERED (From - To)	
4. TITLE AND SUBTITLE Interior and Exterior Laser-Induced Fluorescence and Plasma Potential Measurements on a Laboratory Hall Thruster (Postprint)				5a. CONTRACT NUMBER	
				5b. GRANT NUMBER	
				5c. PROGRAM ELEMENT NUMBER	
6. AUTHOR(S) W. A. Hargus, Jr. and M.A. Cappelli (Stanford Univ.)				5d. PROJECT NUMBER	
				5e. TASK NUMBER	
				5f. WORK UNIT NUMBER	
7. PERFORMING ORGANIZATION NAME(S) AND ADDRESS(ES) Air Force Research Laboratory (AFMC) AFRL/PRSS 1 Ara Road. Edwards AFB CA 93524-7013				8. PERFORMING ORGANIZATION REPORT NUMBER AIAA-99-2721	
9. SPONSORING / MONITORING AGENCY NAME(S) AND ADDRESS(ES) Air Force Research Laboratory (AFMC) AFRL/PRSS 1 Ara Road Edwards AFB CA 93524-7013				10. SPONSOR/MONITOR'S ACRONYM(S)	
				11. SPONSOR/MONITOR'S NUMBER(S) AIAA-99-2721	
12. DISTRIBUTION / AVAILABILITY STATEMENT Approved for public release; distribution unlimited.					
13. SUPPLEMENTARY NOTES Presented at the 35 th AIAA/ASME/SAE/ASEE Joint Propulsion Conference, Los Angeles, CA, 20-24 June 1999. AIAA-99-2721.					
14. ABSTRACT In this paper, we describe the results of a study of laser induced fluorescence velocimetry of ionic xenon in the plume and interior acceleration channel of a laboratory Hall type thruster operating at powers ranging from 250 to 725 W. Optical access to the interior of the Hall thruster is provided by a 1 mm axial slot in the insulator outer wall. Axial ion velocity profiles for four discharge voltages (100 V, 160 V, 200 V, 250 V) are measured as are radial velocity profiles in the near field plume. Internal neutral xenon axial velocity profiles are also measured at these conditions. For comparison, the plume plasma potential profile is measured with an emissive probe. These probe based potential measurements extend from 50 mm outside the plume to the near anode region for all but the highest discharge voltage condition. For each condition, the axial electric field is calculated from the plasma potential. In addition, an estimate of the local electron temperature is calculated from the Bohm criterion at the location of each plasma potential measurement.					
15. SUBJECT TERMS					
16. SECURITY CLASSIFICATION OF:			17. LIMITATION OF ABSTRACT	18. NUMBER OF PAGES	19a. NAME OF RESPONSIBLE PERSON
a. REPORT	b. ABSTRACT	c. THIS PAGE			19b. TELEPHONE NUMBER (include area code)
Unclassified	Unclassified	Unclassified	SAR	16	N/A

AIAA-99-2721

**Interior and Exterior Laser-Induced
Fluorescence and Plasma Potential
Measurements on a Laboratory
Hall Thruster**

W.A. Hargus, Jr. and M.A. Cappelli
Mechanical Engineering Department
Thermosciences Division
Stanford University
Stanford, CA 94305

**35th AIAA/ASME/SAE/ASEE Joint Propulsion
Conference and Exhibit
20-24 June 1999
Los Angeles, California**

Interior and Exterior Laser-Induced Fluorescence and Plasma Potential Measurements on a Laboratory Hall Thruster

W.A. Hargus, Jr.* and M.A. Cappelli
Mechanical Engineering Department
Thermosciences Division
Stanford University
Stanford, CA 94305

Abstract

In this paper, we describe the results of a study of laser induced fluorescence velocimetry of ionic xenon in the plume and interior acceleration channel of a laboratory Hall type thruster operating at powers ranging from 250 to 725 W. Optical access to the interior of the Hall thruster is provided by a 1 mm axial slot in the insulator outer wall. Axial ion velocity profiles for four discharge voltages (100 V, 160 V, 200 V, 250 V) are measured as are radial velocity profiles in the near field plume. Internal neutral xenon axial velocity profiles are also measured at these conditions. For comparison, the plume plasma potential profile is measured with an emissive probe. These probe based potential measurements extend from 50 mm outside the plume to the near anode region for all but the highest discharge voltage condition. For each condition, the axial electric field is calculated from the plasma potential. In addition, an estimate of the local electron temperature is calculated from the Bohm criterion at the location of each plasma potential measurement.

Introduction

Due to their high specific impulse and high thrust efficiencies, Hall thrusters are now being considered for use on commercial, research, and military spacecraft. This technology provides economic advantages for a number of missions and its use can be translated into lower launch mass, longer time on station, or larger payloads [1].

There is a need for increased understanding of the complex phenomena that govern the operation of Hall thrusters. In order to more fully understand the physics in these discharges, several laboratory model Hall thrusters have been constructed at Stanford University. These thrusters have served as test articles for model development and advanced plasma diagnostics including emission, laser induced fluorescence (LIF), probes of various types, as well as thrust measurements [2-7].

Laser based techniques have been developed to nonintrusively probe neutral and ionized xenon [6,7]. Such measurements in the plumes of Hall and other types of ion thrusters provide information on the plasma discharge that is useful in developing insight into the physical processes occurring within these devices. Similar optical diagnostic measurements have been previously

employed to examine plasma properties in other electric propulsion devices. For example, the hydrogen arcjet has been extensively studied using lasers to measure velocity, temperature, and electron number density [8]. The high spatial resolution of single point laser-induced fluorescence is essential in probing nonuniform plasma environments such as those in Hall thrusters and other electric propulsion devices.

Theory

Laser Induced Fluorescence

The interaction of a laser beam with a plasma may involve the optical excitation of a number of atoms to a higher energy state. The excitation is more likely to occur if the laser is tuned to the energy difference $h\nu_{12}$ between an upper and lower excitation level. The interaction can be investigated by either monitoring the resulting reduction in laser power following propagation through the plasma (absorption process), or by monitoring the subsequent spontaneous emission as the resulting excited state relaxes to a lower state (laser-induced fluorescence, LIF). Monitoring the fluorescence as the laser is tuned over the transition provides a measure of the fluorescence excitation line shape and is favored for the higher spatial resolution that it

* Now located at
Air Force Research Laboratory
Spacecraft Propulsion Branch
Edwards AFB, CA

affords in the determination of plasma parameters. The spatial resolution for LIF is determined by the intersection of the probe laser beam with the optical collection volume.

If an absorber has a velocity component u along the axis of the laser beam, it will absorb the light at a frequency shifted from that of stationary absorbers due to the Doppler effect. The magnitude of this frequency shift depends on the velocity along the laser beam axis by,

$$\delta\nu_{12} = \nu_{12} \frac{u}{c} \quad (1)$$

where c is the speed of light. The Doppler shift of a species' fluorescence profile away from the line center ν_{12} of stationary absorbers is in proportion to the species velocity.

The measured fluorescence signal is given by [9-11]

$$S_f = \eta_d \alpha_c h \nu_{12} A_{21} N_2 \quad (2)$$

where η_{12} is the efficiency of the detection system, α_c accounts for factors involving the collection system, and A_{21} is the Einstein coefficient for spontaneous emission of the relevant transition. For low laser intensities, rate equation analysis indicates that the upper level population N_2 , and therefore the fluorescence signal, is linearly dependent on laser intensity at steady state, i.e.,

$$N_2 \sim I_\nu B_{12} \phi_\nu \quad (3)$$

where I_ν is the spectral irradiance at frequency ν , B_{12} is the Einstein stimulated absorption coefficient, ϕ_ν is the transition's spectral line shape which accounts for the variation of the absorption or laser excitation with frequency. The line shape is determined by the environment of the absorbing atoms, so an accurate measurement of the line shape function can lead to the determination of various plasma parameters. However, for velocity measurements, partially saturated fluorescence with a distorted line shape is still capable of providing a reasonable measure of the mean ion velocity. This was experimentally verified with two saturation studies which also examined velocity. The variation of the velocities were found to be less than the experimental uncertainty for the ions (± 500 m/s), or for the neutrals (± 60 m/s).

The line shape is an intrinsic property of the absorbers, whereas the fluorescence excitation line shape is the variation in the detected fluorescence signal with frequency as the laser is tuned across the absorption line feature. If the laser excitation significantly perturbs the populations in the coupled levels, it is said to be saturating the transition and the fluorescence signal is then a nonlinear function of laser intensity. In cases where the laser intensity is significantly below the saturation level and the laser linewidth is small compared to the measured linewidth, the fluorescence excitation line shape reflects the spectral absorption line shape as given by Eqns. 2 and 3. When the laser intensity is sufficiently high to saturate the transition, the fluorescence excitation line shape is broader than the spectral line shape and the fluorescence intensity is less than it would be if it were linear with the laser intensity I_ν . The saturation intensity, defined as that intensity which produces a fluorescence signal half of what it would be if the fluorescence was linear with I_ν , depends inversely on the line strength of the particular line. Stronger transitions have a smaller saturation intensity and thus a larger saturation effect for a given laser intensity.

Xenon Spectroscopy

The ground state of the xenon atom is not easily accessible to LIF. With available laser wavelengths, it is advantageous to probe the excited states. The spectroscopy of the neutral and ionic transitions examined in this study are discussed elsewhere [12-14]. The seven xenon isotopes each have a slight difference in their transition energies due to their differences in mass. The odd mass isotopes are further spin split due to nuclear magnetic dipole and nuclear electric quadrupole moments.

For example, the isotopic and nuclear-spin effects contributing to the hyperfine structure of the $6s[3/2]_2^0 - 6p[3/2]_2$ neutral xenon transition at 823.2 nm produce 21 individual lines. Similarly, the $5d[4]_{7/2} - 6p[3]_{5/2}$ ionic xenon transition at 834.7 nm has a total of 19 isotopic and spin split components. The hyperfine splitting constants are only known for a limited set of levels. The neutral 823.2 nm transition has all of these measured and tabulated in the literature. The ionic 834.7 nm transition only has data on the nuclear spin splitting of the upper state and no available information on the transition dependent isotope shifts [15,16].

For LIF measurements primarily aimed at determining velocities within the plasma flow, it is

often convenient to probe more accessible transitions for which there is incomplete knowledge of the isotopic and nuclear spin splitting constants. Manzella has shown that the ionic xenon transition at 834.7 nm can be used to make velocity measurements in the plume of a Hall thruster [14,17]. An additional convenient feature of this transition is a strong line emanating from the same upper state. This transition at 541.9 nm allows for nonresonant fluorescence collection.

Plasma Potential Measurements

When an electrically isolated conductor is placed in contact with a plasma, the conductor will generally float at a potential ϕ_f other than the plasma potential [18]. The more mobile electrons are depleted near the surface and the resulting electron retarding sheath causes the conductor to float at a potential lower than the plasma potential ϕ_p . One method to measure the plasma potential is to heat a probe until a sufficient number of electrons are thermionically emitted from the probe surface to neutralize the sheath. With the sheath neutralized, the probe will float at the local plasma potential. An advantage of using an emissive probe rather than a swept probe is the issue of cleanliness. Oxide layers on swept probes are difficult to remove and distort the current-voltage characteristic making interpretation of swept probe data difficult.

The relationship between the plasma potential and the floating potential can be used to estimate the electron temperature T_e for a collisionless plasma by equating the ion and electron fluxes [7]. Several assumptions are necessary. First, the ion flux is assumed to be constant. Second, the electron flux to the surface is retarded by a sheath. This sheath is assumed to affect only the electrons which have significantly lower masses than the ions. An estimate for the sheath edge ion velocity is obtained from the Bohm criterion. Strictly, this assumption only applies to a collisionless sheath where ion transport is dominated by the interaction between the plasma and the probe. In the steady state case of a floating conductor in a plasma, the difference between the plasma and floating potentials can be determined by equating the ion and electron fluxes and estimating the electron and ion speeds. The result is

$$\phi_f - \phi_p = -\frac{kT_e}{e} \ln \left[\frac{M}{2\pi m_e} \right]^{1/2} \quad (4)$$

where k is Boltzman's constant, M is the ionic mass, m_e is the electron mass, and e is the elementary charge. With Eqn. 4, measurements of the plasma and floating potentials yield an approximate measure of the electron temperature. Finally, if the plasma potential field is sufficiently well known, it can be numerically differentiated to yield the electric field \vec{E} .

Test Apparatus

Hall Thruster

The thruster used in this study has been described extensively elsewhere [7]. It has 4 outer magnetic windings consisting of 89 mm long, 25 mm diameter cores of commercially pure iron wrapped with 6 layers of 22 gauge insulated copper magnet wire. The inner core is also 25 mm in diameter and 89 mm in height and has 12 layers of magnet wire. The depth of the electrical insulator is 84 mm. The insulator is constructed from 2 sections of cast 99.9% alumina tubing cut to length. These two pieces are cemented to a machinable alumina plate attached to the back plate of the thruster with non-conducting fasteners. A photograph of the assembled thruster is shown in Fig 1.

A second insulator was constructed for the modified Hall thruster. It is identical to the insulator described above with a slot approximately 1 mm wide along the length of the outer wall of cast alumina cut with a diamond saw prior to assembly. The slot is used to provide optical access to the interior of the Hall thruster. Operation of the Hall thruster with the slotted insulator does not appear to differ significantly from the operation with the unslotted insulator. The current voltage characteristics are identical and there are no apparent differences in

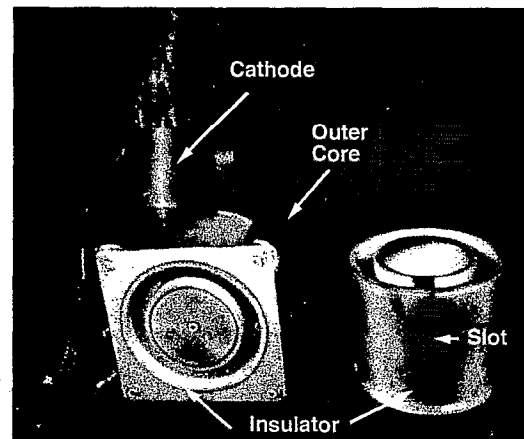


Fig. 1. Photograph of Hall thruster with slotted insulator beside it.

thruster operation. A photograph of the slotted insulator is also shown in Fig. 1. Here, the insulator is shown after testing has been completed. The dark deposits on the insulator are the result of the partial carbonization of the phenolic thruster mount.

The optical access provided by the slot is blocked near the exit plane by the front plate of the magnetic circuit. The front plate is not cut since this would modify the local magnetic field. The magnetic field is one of the most important parameters determining the behavior of the plasma in the Hall thruster and any change in the field would immediately change the characteristics of the plasma. It is felt that the 4 mm field of view blocked by the front plate of the magnetic circuit is less important than preserving the uniformity of the magnetic field within the Hall thruster.

The thruster is mounted on a two axis translation system. In the vertical, the thruster has a range of travel of approximately 30 cm. In the axial, or horizontal, direction, the thruster is constrained to a total travel of approximately 6 cm. Both stages have resolutions on the order of 10 μm , although the repeatability is considerably coarser. For internal LIF measurements with the slotted insulator, the thruster was mounted on a platform supported by the axial translation stage and a linear ball bearing pillow block which provides unimpeded optical access.

Laser Induced Fluorescence

The experimental apparatus used for the laser induced fluorescence measurements consists of a tunable Coherent 899-21 single frequency titanium sapphire laser. The laser is actively stabilized to provide line widths on the order of 1 MHz with near zero frequency drift. Scan widths of up to 20 GHz can be realized at center wavelengths between 680 to 1060 nm. The titanium sapphire laser is pumped by Coherent solid state Verdi pump laser. The pump laser provides 5 W of single mode pump power at 532 nm. The laser wavelength was monitored by a Burleigh Instruments WA-1000 scanning Michelson interferometer wavemeter with a resolution of 0.01 cm^{-1} . Figure 2 shows a schematic of the laser configuration.

The probe beam is directed into the Hall thruster plume by a series of mirrors. The slightly divergent beam (1.7 milliradians full angle) is focused to a submillimeter beam waist by a 50 mm diameter, 1.5 m focal length lens. For radial veloc-

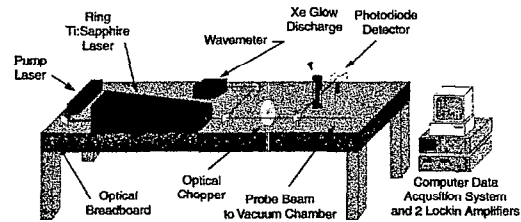


Fig. 2. LIF velocimetry apparatus with laser system and collection optics.

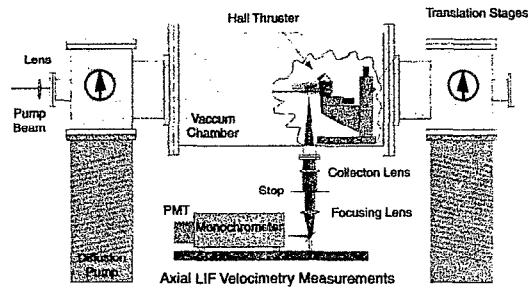


Fig. 3. Stanford high vacuum facility and LIF collection optics with cutaway view of Hall thruster.

ity measurements, the probe beam enters through a side window and is focused by a 50 mm diameter, 50 cm focal length lens. The collection optics for both radial and axial velocity measurements consist of a 75 mm diameter, 60 cm focal length, collimating lens. The collected light is then focused on to the entrance slit of a 0.5 m Ebert-Fastie monochromator with a 50 mm diameter, 30 cm focal length, lens. An optical field stop is placed between the two lenses to match the $F/\#$ of the optical train with that of the monochromator. A schematic of the collection optical train is shown in Fig. 3. The monochromator is used as a narrow band optical filter so that only light from the transition of interest is collected. With entrance and exit slits full open ($425\text{ }\mu\text{m}$), the 600 groove/mm plane grating blazed for 600 nm within the monochromator allows the Hamamatsu R928 photomultiplier tube (PMT) to sample a wavelength interval of approximately 1 nm. The orientation of the monochromator allows the height of the slits to define the length of the probe beam along which the fluorescence is collected. The sample volume for all data presented in this work is approximately $100\text{ }\mu\text{m}$ in diameter and 2 mm in length. Prior to each test and with the PMT housing removed, a HeNe laser is reversed through the entire collection optical train to insure the alignment with the probe beam. For neutral LIF velocimetry measurements, a portion of the probe beam is split from the main beam, passed through a xenon glow discharge tube, and used as an stationary

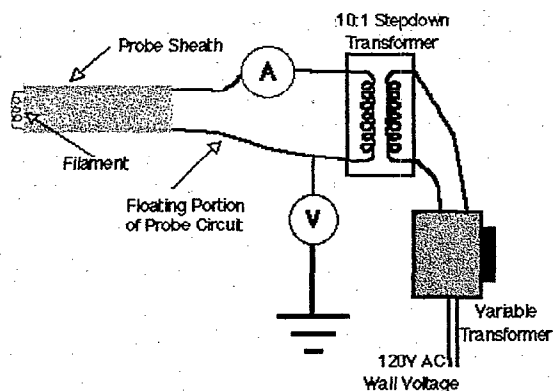


Fig. 4. Plasma potential probe circuit schematic.

absorption reference. A silicon photodiode monitors the absorption signal. This use of the glow discharge tube is only possible for neutral xenon. The glow discharge does not support a sufficient population of excited state ions.

The LIF signal is collected using a Stanford Research Systems SRS-850 digital lockin amplifier. The probe beam is chopped by an SRS-540 optical chopper. The absorption signal from the stationary reference is collected using an SRS-530 lockin amplifier. Data from the absorption signal, laser power output, and the wavemeter are stored on the SRS-850 using 3 available analog inputs along with the LIF signal. Typical tests consist of a 12-20 GHz scan of the probe laser frequency over a 3 minute period. The beam is chopped at a frequency of 1.5 kHz. Both lockin amplifiers use 1 s time constants. Data is sampled at 8 Hz, producing four traces of approximately 2,000 points for each velocity data point. Several unsaturated traces using lower laser intensities, 10 s time constants, and 10 min scans were also performed.

Plasma Potential Probe

The plasma potential probe is constructed from 150 μm diameter 2% thoriated tungsten wire and is described in more detail elsewhere [7]. The filament is formed by winding the thoriated wire around a 0.9 mm mandrel for 8 turns for a total length of approximately 1 cm. The filament is suspended between two 0.50 mm diameter tantalum leads with a separation of 5 mm. The tantalum wires are sheathed in a 6 mm diameter multibore mullite tube. The probe is similar to those used in previous Hall thruster studies [19].

Figure 4 shows a schematic of the probe electrical circuit. The probe is heated using a 10:1 step down transformer powered by a 10 A Power-

stat manual variable transformer connected to wall current (120 V, 60 Hz) which transfers AC power to the probe while allowing the probe circuit to float at the plasma potential.

Test Facility

The Stanford high vacuum test facility consists of a non-magnetic stainless steel vessel approximately 1 m in diameter and 1.5 m in length. The facility is pumped by two 50 cm diffusion pumps backed by a 425 l/s mechanical pump. Base pressure of the facility with no flow is approximately 10^{-6} Torr as measured by an ionization gauge uncorrected for gas species. Chamber pressures during thruster testing at xenon flow rates of approximately 2.3 mg/s result in chamber background pressures of in the region of 10^{-4} Torr. This indicates that the facility has a xenon pumping speed of approximately 2,000 l/s. Propellant flow to the thruster anode and cathode is controlled by two Unit Instruments 1200 series mass flow controllers factory calibrated for xenon. The propellant used in this study was research grade (99.995%) xenon. The thruster was mounted on two translation stages which allowed motion in the vertical and axial directions. A schematic of the facility with the Hall thruster mounted is shown in Fig. 3.

Results and Analysis

Operating Conditions

The Hall thruster was operated at four conditions. At each of these conditions, the peak magnetic field was measured to be approximately 125 G, the mass flow to the anode was 2 mg/s, mass flow to the cathode was 0.3 mg/s. The test conditions corresponded to discharge voltages of 100, 160, 200, and 250 V. The anode currents for these conditions were 2.1, 2.4, 2.6, and 2.9 A, respectively. The total power consumed by the cathode and magnet circuit was approximately 30 W. It should be noted that the power dissipated in the ballast resistors on the anode and cathode keeper lines (~ 10 W) are not included in these calculations.

Position Reference

All spatially resolved measurements are referenced to a two coordinate system. The position in the radial coordinate is referenced to the difference of the radial location and the radial location corresponding to the acceleration channel center using the variable D which is defined as positive toward the thruster centerline. The axial coordinate is given by Z which is the distance from the

thruster exit plane and is defined as positive along the thrust vector.

Ionic LIF Velocimetry

The axial LIF velocimetry data consists of two sets of measurements taken with the slotted insulator. The first set consists of ionic velocity measurements taken externally extending from the exit plane to approximately $Z = 35$ mm. The second set of data points consist of internal axial velocity data from the exit plane to approximately $Z = -65$ mm. These limits are imposed by the limited range of the translation stage providing axial motion of the Hall thruster. Between each data set, the transla-

tion stages had to be repositioned so that the subsequent data set could be taken. Data points were taken every 2.5 mm with a sample probe volume $100\text{ }\mu\text{m}$ in diameter and 2 mm long. Overlap of the two data traces ensure that the measurements are continuous. For several of the test conditions examined, profiles of the axial velocity across the coordinate D are also examined.

The complete axial velocity profiles for the four cases examined are shown in Fig. 5. The error bars correspond to the uncertainty associated with the determination of the magnitude of the Doppler shift (500 m/s). The axial velocity profiles exhibit a typical behavior. The velocity is near zero near the anode ($Z = -78$ mm), and begins to rise near $Z = -10$ mm. The ions are rapidly accelerated in the region of the exit plane and reach their full velocity in the neighborhood of $Z = 20$ mm. This latter position corresponds to the location of the hollow cathode neutralizer relative to the body of the thruster and is often referred to as the *cathode plane* in the literature [14].

The length of the acceleration region for each case shown is invariant at 30 mm. Therefore, increases in the anode potential result in linearly increased electric fields within the thruster acceleration channel. The initial acceleration begins 10 mm within the thruster where the magnetic field has a value of approximately 85% of the centerline ($D = 0$) maximum. The propellant acceleration is completed 20 mm beyond the exit plane when the magnetic field has a value of approximately 25% of the centerline maximum.

Significant acceleration occurs outside the Hall thruster. Taking into account the uncertainties inherent to the velocity measurements (± 500 m/s), the velocity increment imparted into the propellant outside the Hall thruster is essentially constant with an average value of 5,000 m/s. Only for the case of a 100 V discharge voltage, does the majority of the acceleration occur outside the thruster. Higher discharge voltages appear to have a constant percentage of the acceleration occurring externally. It is also informative to examine the energy deposited into the propellant. In the case of a 100 V discharge voltage, approximately 90% of the energy is deposited into the propellant beyond the exit plane. For all cases above 160 V discharge voltage, the fraction of energy deposition beyond the exit plane is nearer to 60%. Thus, the majority of the energy deposition into the Hall thruster propellant stream

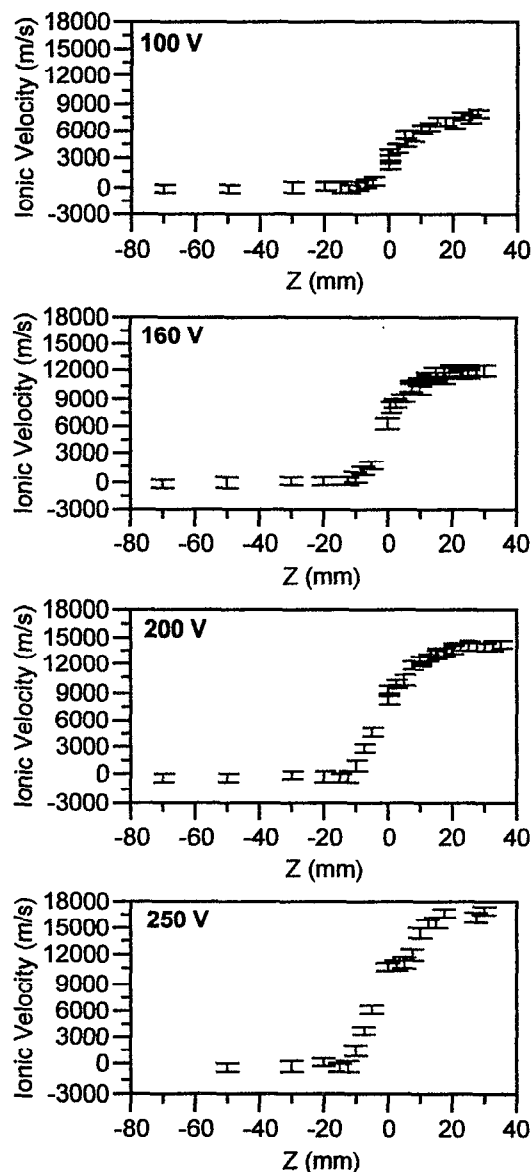


Fig. 5. Axial ionic velocity measurements at $D = 0$ mm for 4 discharge voltage conditions.

occurs outside the thruster body. However since the thrust is equivalent to the momentum flux, the majority (65%) of the thrust is still generated within the thruster body in all cases but that of the 100 V discharge voltage. In all the cases, approximately 60 eV appear to not contribute to the propellant acceleration. This value is constant to within the uncertainties of the velocity measurements and implies that the mechanism responsible for this loss is invariant with the applied anode potential. This energy loss is therefore most likely a product of the anode and cathode potential falls and other mechanisms inherent to the thruster design. It must be noted that the measurements presented thus far are limited to axial velocities and can not account for losses due to plume divergence.

Several radial profiles of the axial ionic velocity in Fig. 6 illustrate the radial variation of the measured axial velocities for a discharge voltage of 160 V at two locations in the plume and within the thruster for a discharge voltage of 200 V. The width of the acceleration channel is approximately 12 mm ($-6 \text{ mm} < D < 6 \text{ mm}$) and it is quite evident that the plume is sufficiently diverged at the axial locations examined such that the axial velocity profile is flat which strongly implies lines of constant potential in the radial direction.

Radial velocity measurements were performed in the plume. Combined with the above axial velocity measurements with the knowledge that the axial velocity appears to be independent of D , vector plots of the near plume may be constructed. Figure 7 shows a vector plot constructed for a 200 V discharge voltage. In this case, radial velocities vary linearly with D with near zero velocity at $D = 0 \text{ mm}$ and peak at values above 6,000 m/s

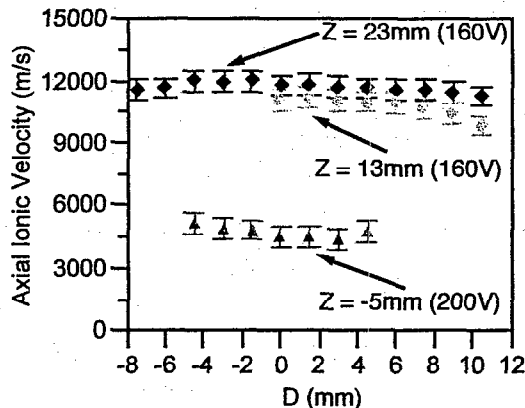


Fig. 6. Profiles of the axial ionic velocity for several discharge voltages and locations.

as close as $Z = 13 \text{ mm}$ and $D = 8 \text{ mm}$. A strong feature of a Hall thruster plume is the central core of the plume. The propellant stream exits the thruster in an annulus, but a intense, optically emitting conical feature starting near the central magnetic core and extending a distance into the vacuum chamber is especially evident at higher discharge voltages and extends several meters in vacuum facilities with lower background pressures than those available at Stanford University. This inward focus of the divergent propellant flow likely accounts for this commonly observed plume structure.

Ionic Line Shape Analysis

The hyperfine splitting constants for the ionic xenon $5d[4]_{7/2} - 6p[3]_{5/2}$ transition at 834.7 nm are only known for the upper $6p[3]_{5/2}$ state. Similarly, the isotope shifts for this transition are unknown. In addition to the lack of spectroscopic information, the plasma environment introduces uncertainties in the determination of an ionic kinetic temperature from an unsaturated line shape. First, the time averaged broadening of the excitation spectra can not be due to plasma oscillations. King has shown in energy analyzer studies that the axial velocity of the exiting ions have an energy distribution of approximately 10 eV due to the plasma oscillations within the Hall thruster [20]. Second, the low density of the plasma may preclude a Maxwellian velocity distribution among the ions. If so, the concept of a kinetic temperature is not valid. The issue of the distribution of ionic velocities is minimized by examining the fluorescence spectra in the radial direction. The spectra is taken from the position with the minimum measured velocity,

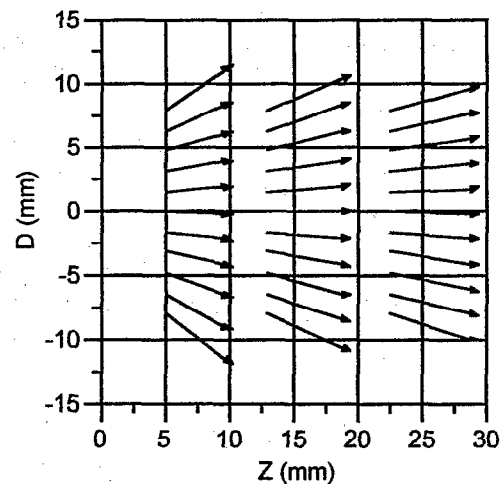


Fig. 7. Estimated flow vectors from radial velocity measurements for a 200 V discharge voltage.

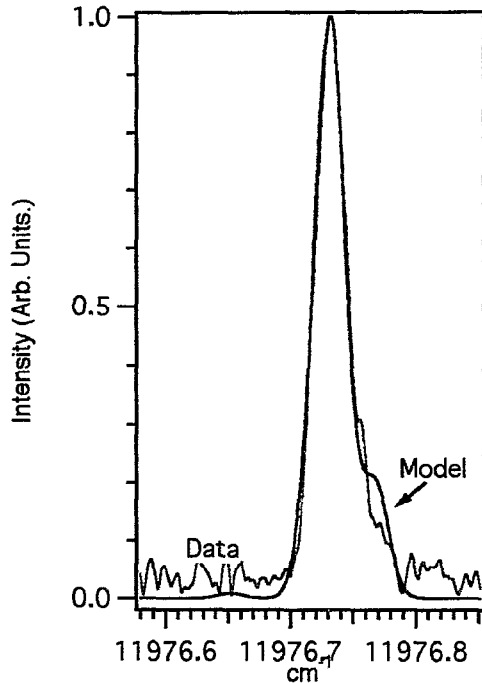


Fig. 8. Model fit to unsaturated fluorescence trace at 200 V, D = 0 mm, and Z = X mm.

approximately 100 m/s at a location of D = 0 mm and Z = 13 mm. The ion population is assumed to be Maxwellian, or at least frozen into a close facsimile.

Despite the inherent limitations, an estimate of the kinetic temperature is still possible if uncertainties of 40-70% are acceptable [21]. An unsaturated fluorescence trace is shown in Fig. 8 and compared to a model developed by Cedolin [22]. The model uses the $5d[3]_{7/2}$ lower level hyperfine spin splitting and isotopic shift data from the 605.1 nm transition and the measured splitting data for the upper $6p[3]_{5/2}$ level. Lorentzian broadening is neglected and only Doppler broadening is considered. The best fit of this model predicts a kinetic temperature of approximately 450 K. The model still does not completely predict the outlying features, but this is expected since the incorrect spin splitting constants are used for the lower level. As a final note on the uncertainty of this model, if hyperfine splitting is ignored and only the isotope shifts corresponding to the values for the 605.1 nm transition are used, the model predicts a kinetic temperature of approximately 750 K.

The kinetic temperature of the ions is between 450 and 750 K. The uncertainty of this

measurement is in large part due to the uncertainties of the spectral data as well as due to the noise in the fluorescence signal. A similar measurement in the plume of a SPT-100 by Manzella yielded a kinetic temperature of approximately 800 K [14]. It should be noted that Manzella used the incorrect value of the electron angular momentum J for the lower state that was first misidentified by Humphreys [23] and propagated by Moore [24] before finally being corrected by Hansen and Persson [17]. This may account for the slightly higher kinetic temperature; although, the uncertainty is such that the difference in the temperatures is probably inconsequential.

Neutral LIF Velocimetry

Figure 9 shows axial neutral velocity measurements within the acceleration channel of the Hall thruster. All four cases examined show very similar behavior. The initial velocity near the anode is very low. The neutral velocity slowly rises until a position approximately 20 mm within the thruster. At this point where the ion acceleration also begins, the neutrals are accelerated at a higher rate until near the exit plane where the acceleration appears to slow and even reverses when the thruster is operated at discharge voltages of 200 V, or above. The decrease in the neutral velocity is best explained by the thruster ingestion of background neutral xenon. Since the effect appears to grow with increased discharge voltage, it is possible that a portion of the flow reflected from nearby vacuum facility walls is ingested by the thruster. Once the background neutral xenon is in the vicinity of the discharge, the high electron density near the exit plane will collisionally excite the background atoms. Some of these atoms will be ionized and the external electric fields produced by the thruster will accelerate the resulting ions downstream, albeit with lower final energies than ions created within the thruster. Some of the atoms will be electronically excited, but not be ionized and will optically decay to the $6s[3/2]_2^0$ metastable level where they could be sampled during neutral LIF velocimetry measurements.

Flow from the cathode can be eliminated as the source of the apparent slowing down of the neutrals for several reasons. First, the flow from the cathode, although 15% of the anode flow, is exiting from a 2 mm orifice approximately 12 cm above the sample volume. Flow from the cathode should be sufficiently diffused and not affect the neutral velocity measurements. Second, the cathode is angled 30° from the front plate pointed down-

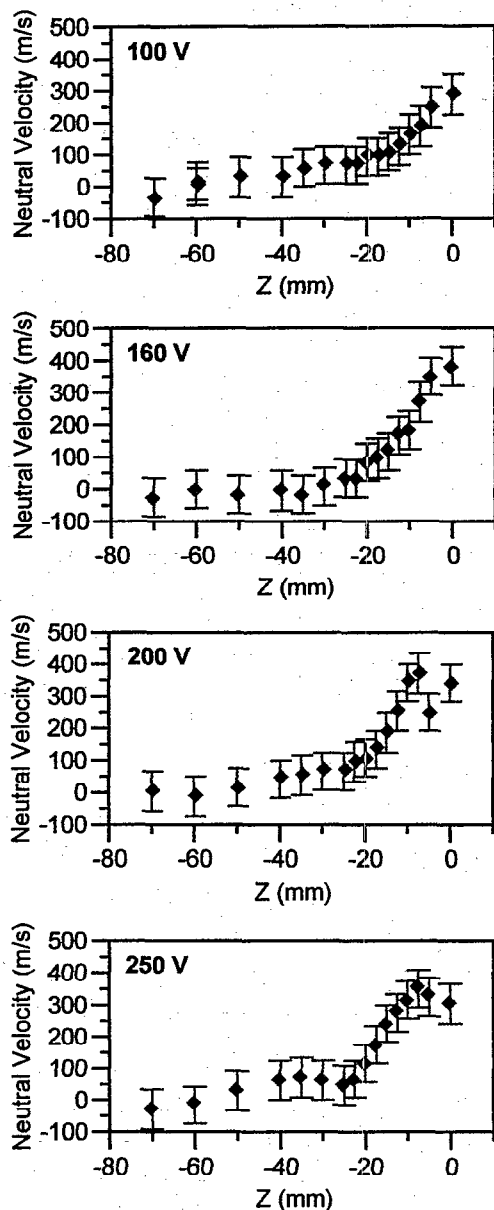


Fig. 9. Axial neutral velocity measurements at $D = 0$ mm for several conditions.

stream. It is difficult to see how flow from the cathode could affect neutral velocity measurements within the acceleration channel. It is therefore almost certain that random neutral flux from the chamber background is responsible for the apparent drop in neutral velocity seen near the exit plane in Fig. 9.

Due to the highly nonequilibrium nature of the Hall thruster, it is important to understand the apparent acceleration of the neutrals. The plasma within the Hall thruster is required to be very dif-

fuse by the constraint that the magnetic field restrain the electron flux to the anode. This requirement appears to be in force when the neutral velocity measurements are compared with the ionic velocity measurements. The disparate velocities of the ions and neutrals strongly suggest that the neutral and ion populations are not coupled. As such, the apparent acceleration of the neutrals may actually be an artifact of the time of flight of the neutrals through the volumetric zone of ionization. Slower neutrals, or neutrals that travel a longer effective path length due to collisions with the walls of the acceleration channel, have a proportionally greater chance being ionized than do neutrals in the high energy portion of the velocity distribution. Therefore, neutrals from the high energy tail of the velocity distribution are more likely to reach the upstream portions of the acceleration channel. In this case, there is no actual acceleration of the neutrals, but rather a depletion of the slower moving neutrals by ionization.

Plasma Potential Measurements

Since Hall thrusters are electrostatic accelerators, knowledge of the plasma potential is important in understanding the propellant acceleration process. The correspondence between the ion velocity measurements and the plasma potential measurements provides an indication of the efficiency of the propellant acceleration process.

Figure 10 shows the measured axial plasma potential and electron temperature estimated using the Bohm criterion for the four conditions examined. Each data trace shows similar behavior where the potential is constant in the far plume near a value of 25 V, likely corresponding to the potential of the electrons produced by the hollow cathode neutralizer and impedance produced by any residual magnetic field in the plume. As the probe traverses into the thruster acceleration channel, the potential rises significantly as the impedance of the radial magnetic field to the axial electron current is encountered. The plasma potential rapidly rises and by $Z = -20$ mm has reached 80-90% of the anode potential. The remaining 10-20% of the potential is distributed between this position and the anode and does not appear to accelerate the ions. The 250 V case is incomplete due to failure of the probe where the tantalum leads melted and the thoriated tungsten filament lost electrical contact with one, or both, of the leads. No measurements further into the acceleration channel were possible for a discharge voltage of 250 V.

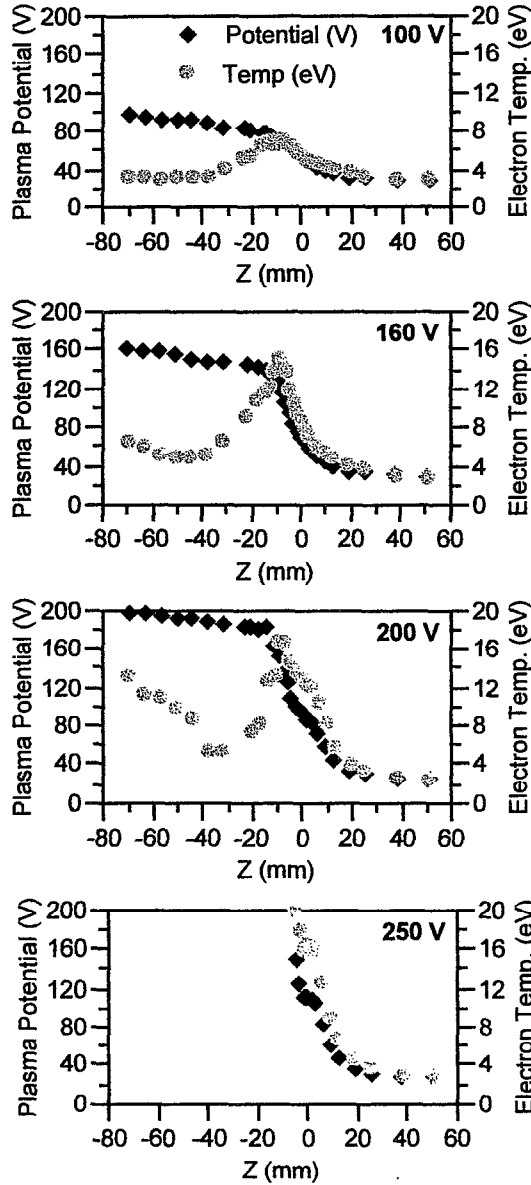


Fig. 10. Axial plasma potential and estimated electron temperatures at $D = 0$ mm at several discharge voltages.

An estimate of the electron temperature is also shown in Fig. 10. The general behavior is an electron temperature at a low value (2.5-3 eV) in the plume which rises with the rising plasma potential to a maximum located between $Z = -8$ and -10 mm. The electron temperature then begins to fall even though the plasma potential is only at 80% of the anode potential. The rapid fall off of the electron temperature occurring between $Z = -10$ to -40 mm is primarily due to a rapidly rising floating potential. Closer to anode ($Z < -40$ mm), the electron temperature again begins to rise. Here, the

plasma potential is only rising slowly, but the floating potential drops, and as a result, the electron temperature rises. This effect grows significantly more pronounced as the discharge voltage increases. For example at a discharge voltage of 100 V, the electron temperature rise near the anode is nearly imperceptible. At 160 V, the rise in electron temperature is well defined, and at 200 V, the rise in electron temperature near the anode approaches the peak temperatures of the exit plane.

Somewhat similar behavior has been seen in the literature [19]. In this study, a two dimensional potential field of a Hall thruster of similar geometrical dimensions operating on argon at a discharge voltage of 400 V was generated. Strong variation in the radial direction of the plasma potential was found to exist in the 30 mm nearest to the anode within an acceleration channel of 138 mm total length. Similar measurements could not be performed on the Stanford Hall thruster due to geometrical constraints. However, a similar potential field is implied in this case since it would produce electric fields which would heat local electrons to elevated temperatures as is seen in Fig.10.

A typical radial profile of the plasma potential and the derived electron temperature at $Z = 13$ mm is shown in Fig.11. The data show a portion of the structure within the near field plume. The annular ion beam has diffused significantly by this axial location, yet retains a distinct structure. The asymmetry also shows the development of the bright central core feature. The asymmetry manifests itself the greatest at low discharge voltages where the potential near the central magnetic core remains at a higher value than it does toward lesser values of D . This phenomena lessens at higher discharge voltages; however, the absolute magnitude of the potentials within the core and in the outer portion of the plume retain a potential difference of

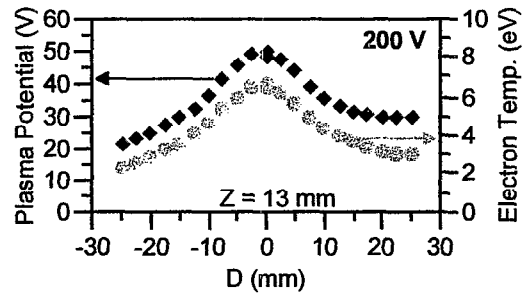


Fig. 11. Radial profile of plasma potential and estimated electron temperature at $Z = 13$ mm at a discharge voltage of 200 V.

nearly 10 V in all cases. Less mixing is occurring as the ionized propellant stream has greater momentum with increased discharge voltage. This explains the extended plume structure seen at the higher discharge voltages. Since the plume structure is also more visible at lower pressures, a portion of the perceived diffusion may in fact be entrained and subsequently ionized background xenon.

The electron temperatures calculated from the radial plasma potential measurements show some of the asymmetry of the plasma potential data, especially at the lower discharge voltages. However, the asymmetry is in general much less pronounced for the electron temperatures than it is for the plasma potentials across D. Otherwise, the electron temperature profile follows the plasma potential profile.

The uncertainty associated with the plasma potential measurements is difficult to quantify. Especially since the measurement only approaches the true plasma potential. The values of the data above have a precision/repeatability of approximately ± 3 V. A study of apparent plasma potential to probe filament current indicates that the measurements are probably within several volts of the true plasma potential [12]. This would indicate an uncertainty associated with the plasma potential measurements of approximately $-3/+6$ V. The related uncertainty of the electron temperature can be calculated from the uncertainty associated with the measurement of the plasma and the floating potentials and is approximately ± 0.5 eV.

Another issue that needs to be addressed is how much the plasma potential probe affected the operation of the Hall thruster. At 100 V, the lowest discharge voltage examined, the discharge current did not appreciably vary during insertion and removal of the probe ($< 8\%$). In all cases, the discharge current did not vary if the probe was heated, or was not. At higher discharge voltages, the discharge current was strongly affected by the position of the 6 mm diameter probe within the acceleration channel. For all cases above 160 V when the probe tip is traversing the first 20 mm within the acceleration channel, the current rises to nearly 130% of the nominal value. Placing the probe significantly further into the thruster only raises the potential less than an additional 10%. Clearly, the probe is perturbing the discharge in the first 20 mm where it has already been determined the acceleration of the ions begins. This effect is not seen at 100 V.

Electric Field Calculations

The axial component of the electric field is extracted for the plasma potential data in Fig. 10, using Eqn. 5 and shown in Fig. 12. Also presented in this figure are values for the electric field calculated by determining the ion kinetic energy from the velocimetry data in Fig. 5 and differentiating to produce an effective electric field. The two data sets show remarkable similarity indicating that the ionization and acceleration regions within the thruster are separated to some degree. The differences between the two sets of curves are due to the differences between the data. Ion creation occurs in a volume and therefore the LIF derived plasma potentials are only valid beyond the region of ion creation which appears to lie near $Z = -10$ mm. Unfortunately, there is probably significant ionization occurring throughout the acceleration channel which accounts for some of the differences. Some ions are likely created in regions where the electric field is high and this masks the detection of local electric fields using velocimetry data, especially if the zone of ion creation is large and the ion velocities are subsequently distributed.

Another issue with determining plasma potentials and electric fields from velocimetry data is that the uncertainties associated with the ionic velocity measurements are magnified by the derivation of potential and subsequent electric field data. With the plasma potential probe, the primary issue is the degree of disturbance by the probe while the LIF velocimetry is non-intrusive, or less intrusive with the addition of the slot in the insulator.

Both data sets show similar trends. Some of the features are different, particularly those more than 10 mm within the Hall thruster exit plane. Between $Z = -10$ mm and the anode, there exists only a small population of ions with low axial velocities with uncertain creation and loss rates. Velocimetry studies prove inadequate to study the potential and electric field in this region, but potential probe measurements, assuming that they do not significantly perturb thruster operation, provide better measurement of the plasma potential and subsequently a better indication of the electric field. It is believed that the probe, undermeasures the higher gradients of the plasma potential due to the probe body perturbing the plasma flow field. This would explain the why the electric fields measured by the probe are somewhat less than those determined from velocimetry studies.

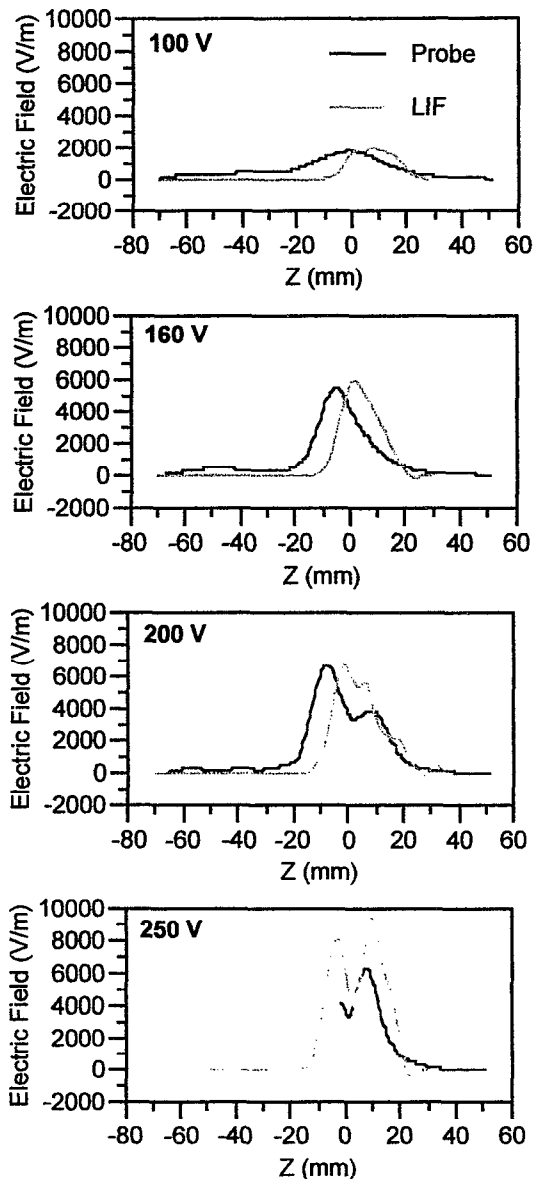


Fig. 12. Comparison of axial electric field calculated from plasma potential and LIF velocimetry data.

It is interesting to note that the trends of both probes agree, particularly near the exit plane where a very low electric field is indicated. This sudden change in the electric field at the exit plane is visible in both data sets and increases with increasing discharge voltage. If it can be assumed that the axial current is a constant and since the local radial magnetic field is continuous, the dips in the electric field can be attributed to changes in the local plasma conductivity indicating either a sharp drop in the electron temperature, or a rise in the electron density. The measured electron temperature does not support the former; therefore, a sharp

rise in the electron density may be responsible. The most likely explanation for a rise in electron density is that due to the high back pressure within the vacuum facility (10^{-4} Torr) there may be a second ionization zone near the exit plane of the thruster. In flowing electrons ionizing background neutrals could produce a higher plasma density in this region thus increasing the local plasma conductivity and lowering the local electric field as seen in Fig. 12.

Figure 13 shows the radial component of the electric field calculated from the radial plasma potential measurements presented in Fig. 11. The magnitude of the electric field peaks at a relatively large value and shows the electrostatic forces focusing/defocusing the plume. The radial electric field peak magnitude increases with discharge voltage from a peak value near 1,000 V/m at 100 V to approximately 2,500 V/m at a discharge voltage of 250 V. The peak value of the radial component of the electric field at this location in the plume is approximately equal to the axial component at this location.

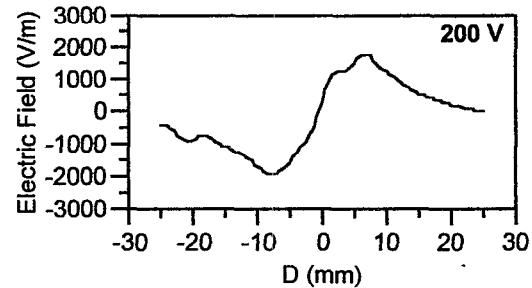


Fig. 13. Radial electric field (relative to D) at $Z = 13$ mm for a discharge voltage of 200V

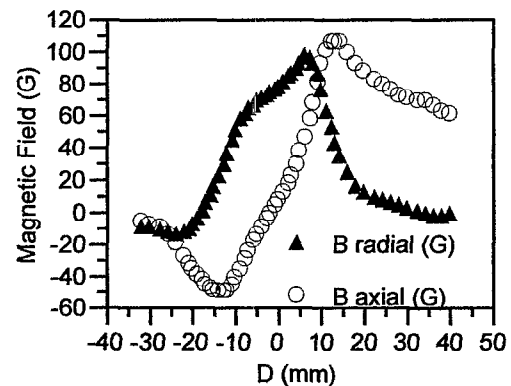


Fig. 14. Plot of thruster magnetic field components at $Z = 3$ mm.

The variation of the radial electric field is similar to the variation seen in the axial component of the thruster magnetic field. The impedance of the plasma, whether either classical or enhanced electron diffusion holds, is a function of the magnetic field strength and also a vector quantity. Figure 14 is a plot of the magnetic field components at $Z = 3$ mm. The variation of the axial portion of the magnetic field is most of interest here. At this position in the plume, the electron temperature does not vary significantly and the electron density appears to be near constant, and therefore, the radial electric field is proportional to the axial magnetic field. The density effect can be seen from the effect of discharge voltage. As the discharge voltage is increased, the velocity of the ion propellant stream rises and the plasma density falls. Along with the fall in plasma density, the conductivity falls and the radial electric field increases.

Conclusions

Measurements ion velocity, neutral velocity, and plasma potentials were performed in the plume and into the interior of the thruster through a 1 mm wide slot in the outer insulator wall. From these measurements, information on propellant energy deposition, electric field strength, electron temperature, and flow divergence were extracted.

Ionic velocity measurements of axial velocity both inside and outside the thruster as well as radial velocity measurements outside the thruster, were performed using LIF with nonresonant signal detection using the ionic xenon $5d[4]_{7/2} - 6p[3]_{5/2}$ excitation transition while monitoring signal from the $6s[2]_{3/2} - 6p[3]_{5/2}$ transition. Neutral velocity measurements were similarly performed in the interior of the Hall thruster using the $6s[3/2]_2^0 - 6p[3/2]_2$ transition with resonance fluorescence collection. Most velocity measurements used saturated transitions to improve the signal to noise ratio. One radial trace of the ionic transition was taken in the linear fluorescence region and yielded an ionic translational temperature between 450 and 750 K. However, since the hyperfine structure constants are not known for the $5d[4]_{7/2}$ level, the constants for the $5d[3]_{7/2}$ level were used instead. This result should therefore be viewed with caution. The ionic velocity data allowed for the measurement of the energy deposited into the propellant stream which was calculated as the kinetic energy of the ions. An effective elec-

tric field was calculated from the ionic kinetic energy.

Plasma potential measurements were made in the plume and interior of the thruster. Unfortunately, the probe perturbs the Hall thruster discharge. However, the perturbation of the discharge could not be avoided if potential measurements were to be made. The potential measurements showed that the far plume was approximately 25 V above ground, probably corresponding the potential of the electrons produced by the hollow cathode neutralizer. Electric field values derived from the plasma potential measurements show that the fields are relatively smooth and peak near the exit plane. Maximum field strengths were found to be approach 8,000 V/m. At the exit plane, the axial electric fields show a dip for nearly all the discharge voltages examined where the plasma potential is near constant. In addition, an estimate of the electron temperature was extracted at the location of each plasma potential measurement. This was done by also measuring the probe floating potential at the same location as each plasma potential measurement.

Acknowledgments

This work is supported by the Air Force Office of Scientific Research. W.A. Hargus, Jr. was supported under the Air Force Palace Knight Program.

References

1. S.W. Janson, "The On-Orbit Role of Electric Propulsion," AIAA-93-2220, 29th Joint Propulsion Conference, 28-30 June 1993, Monterey, CA.
2. R.J. Cedolin, W.A. Hargus, Jr., R.K. Hanson, and M.A. Cappelli, "Laser Induced Fluorescence Diagnostics for Xenon Hall Thrusters," AIAA-96-2986, 32nd Joint Propulsion Conference, July 1-3, 1996, Lake Buena Vista, FL.
3. R.J. Cedolin, W.A. Hargus, Jr., R.K. Hanson, and M.A. Cappelli, "Laser Induced Study of a Xenon Hall Thruster," AIAA-97-3053, 33rd Joint Propulsion Conference July 6-9, 1997, Seattle, WA.
4. W.A. Hargus, Jr., N.B. Meezan, and M.A. Cappelli, "Transient Behavior of a Low Power Hall Thruster," AIAA-97-3050, 33rd Joint Propulsion Conference July 6-9, 1997, Seattle, WA.
5. W.A. Hargus, Jr., R.J. Cedolin, N.B. Meezan and M.A. Cappelli, "A Performance Study of a Low Power Hall Thruster," AIAA 97-3081, 33rd Joint Propulsion Conference July 6-9, 1997, Seattle, WA.

6. R.J. Cedolin, W.A. Hargus, Jr., P.V. Storm, R.K. Hanson, and M.A. Cappelli, "Laser-induced Fluorescence Study of a Xenon Hall Thruster," *Applied Physics B: Lasers and Optics*, Vol. 65, pp 459-469, 1997.
7. W.A. Hargus, Jr. and M.A. Cappelli, "Laser Induced Fluorescence Measurements on a Laboratory Hall Thruster," AIAA-98-3645, 34th Joint Propulsion Conference, 13-15 July 1998, Cleveland, OH.
8. P.V. Storm, *Optical Investigations of Plasma Properties in the Interior of a Arcjet Thrusters*, Thermosciences Division Report No. TSD-102, Ph.D. Dissertation, Stanford University, 1997.
9. R. P. Lucht, "Applications of Laser-Induced Fluorescence Spectroscopy," in *Laser Spectroscopy and its Applications*, edited by L. J. Radziemski, R. W. Solarz, and J. A. Paisner, Marcel Dekker, New York, 1987.
10. A.C. Eckbreth, *Laser Diagnostics for Combustion Temperature and Species*, Overseas Publishers Association, Amsterdam, 1996.
11. W. Demtroder, *Laser Spectroscopy: Basic Concepts and Instrumentation*, Springer-Verlag, Berlin, 1996.
12. W.A. Hargus, Jr. and M.A. Cappelli, "Laser Induced Fluorescence Measurements within a Laboratory Hall Thruster," AIAA-99-3436, 30th Plasma Dynamics and Lasers Conference, June 28 - 1 July, 1999, Norfolk, VA.
13. R. J. Cedolin, R. K. Hanson, and M. A. Cappelli, "Semiconductor Laser Diagnostics for Xenon Plasmas," AIAA-94-2739, 30th Joint Propulsion Conference, June 27-29, 1994, Indianapolis, IN.
14. D.H. Manzella, "Stationary Plasma Thruster Ion Velocity Distribution," AIAA-94-3141, 30th Joint Propulsion Conference, June 27-29, 1994, Indianapolis, IN.
15. L. Bronstrom, A. Kastberg, J. Lidberg, S. Mannervik, "Hyperfine-structure Measurements in Xe II," *Physical Review A*, Vol. 35, No. 1, Jan. 1996.
16. H. Geisen, T. Krumpelmann, D. Neuschafer, and Ch. Ottinger, "Hyperfine Splitting Measurements on the 6265 Å and 6507 Å Lines of Seven Xe Isotopes by LIF on a Beam of Metastable Xe(³P_{0,3}) Atoms," *Physics Letters A*, Vol. 130, No. 4.5, 11 July 1988.
17. J. E. Hansen and W. Persson, "Revised Analysis of Singly Ionized Xenon, Xe II," *Physica Scripta*, Vol. 36, pp 602-643, 1987.
18. M.A. Lieberman and A.J. Lichtenberg, *Principles of Plasma Discharges and Materials Processing*, John Wiley and Sons, Inc., New York, 1994.
19. A.I. Morozov, Y.V. Esipchuk, G.N. Tilinin., A.V. Trofimov, Yu. A. Sharov, and G. Ya. Shshepkin, "Plasma Accelerator with Closed Electron Drift and Extended Acceleration Zone," *Soviet Physics - Technical Physics*, Vol. 17, No. 1, July 1972.
20. L. B. King, *Transport-Property and Mass Spectral Measurements in the Plasma Exhaust Plume of a Hall-Effect Space Propulsion System*, Ph.D. Dissertation, Aerospace Engineering, University of Michigan, June 1998.
21. R. J. Cedolin, Personal Communication, 23 Jan. 1999.
22. R. J. Cedolin, *Laser-Induced Fluorescence Diagnostics of Xenon Plasmas*, Ph.D. Dissertation, Mechanical Engineering, Stanford University, June 1997.
23. C. J. Humphreys, "Second Spectrum of Xenon," *Journal of the National Bureau of Standards*, Vol. 22, Jan. 1939.
24. C. E. Moore, *Atomic Energy Levels: Volume III*, National Bureau of Standards, Washington, 1958.